

See discussions, stats, and author profiles for this publication at: <https://www.researchgate.net/publication/277939910>

# Broadband Light Harvesting and Fast Charge Separation in Ordered Self-Assemblies of Electron Donor-Acceptor-Functionalized Graphene Oxide Layers for Effective Solar Energy Conversi...

ARTICLE *in* THE JOURNAL OF PHYSICAL CHEMISTRY C · MAY 2015

Impact Factor: 4.77 · DOI: 10.1021/acs.jpcc.5b03303

---

CITATION

1

READS

27

## 6 AUTHORS, INCLUDING:



Mustafa Supur

University of Alberta

20 PUBLICATIONS 226 CITATIONS

[SEE PROFILE](#)



Mase Kentaro

Osaka University

16 PUBLICATIONS 109 CITATIONS

[SEE PROFILE](#)



Kei Ohkubo

Osaka University

395 PUBLICATIONS 9,572 CITATIONS

[SEE PROFILE](#)

# Broadband Light Harvesting and Fast Charge Separation in Ordered Self-Assemblies of Electron Donor–Acceptor-Functionalized Graphene Oxide Layers for Effective Solar Energy Conversion

Mustafa Supur,<sup>†</sup> Yuki Kawashima,<sup>†</sup> Kentaro Mase,<sup>†</sup> Kei Ohkubo,<sup>†,||</sup> Taku Hasobe,<sup>‡</sup> and Shunichi Fukuzumi<sup>\*,†,§,||</sup>

<sup>†</sup>Department of Material and Life Science, Graduate School of Engineering, Osaka University, ALCA and SENTAN, Japan Science and Technology Agency (JST), Suita, Osaka 565-0871, Japan

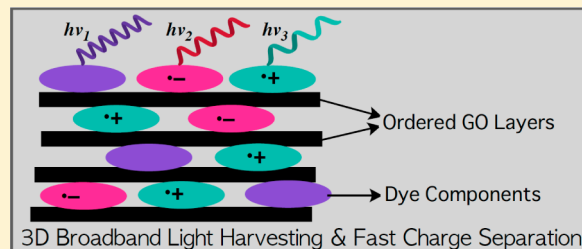
<sup>‡</sup>Department of Chemistry, Faculty of Science and Technology, Keio University, Yokohama, Kanagawa 223-8522, Japan

<sup>§</sup>Faculty of Science and Technology, Meijo University and ALCA and SENTAN, Japan Science and Technology Agency (JST), Tempaku, Nagoya, Aichi 468-8502, Japan

<sup>||</sup>Department of Bioinspired Science, Ewha Womans University, Seoul 120-750, Korea

## S Supporting Information

**ABSTRACT:** Three-dimensionally (3D) ordered assemblies of GO layers functionalized with tetrakis(1-methylpyridinium-4-yl)-porphyrin *p*-toluenesulfonate (Por), *N,N'*-di(2-(trimethylammonium iodide)ethylene) perylenediimide (PDI), and Zn(II) phthalocyanine tetrasulfonic acid (ZnPc) were obtained in water. Proper molar ratio is essential between the cationic dyes, Por and PDI, acting as the “glue” molecules to combine the GO layers and the anionic ZnPc, acting as dispersant of GO layers to (i) construct the 3D assemblies and (ii) the proportional absorption distribution of dye-functionalized GO assemblies. Resulting 3D structures effectively harvest the light from ultraviolet to near-infrared (NIR) regions. Dye molecules are arranged in mainly lateral order on the GO layers with partial stacking, which allows direct interactions with the  $\pi$ -conjugations of the GO surface in 3D architecture. Ultrafast charge separation upon the photoexcitation of the dyes at various wavelengths in the visible/NIR region was observed in these assemblies, in which ZnPc and PDI were the ultimate electron donor and acceptor, respectively. Lateral charge migration among the partially stacked dye molecules was inferred from the decay characteristics of the radical ion pair. Triggered by the charge separation processes in the 3D ordered self-assemblies, significantly higher photocurrent density in the OTE/SnO<sub>2</sub> electrode deposited with self-assemblies of (GO–Por–PDI–ZnPc)<sub>n</sub> was generated compared to those deposited with only GO or dye components.



## 1. INTRODUCTION

Graphene oxide (GO), possessing sp<sup>2</sup>-hybridized carbon patterns principally extending in two dimensions, presents openings for the emergence of new composite materials for photochemical applications.<sup>1–7</sup> Due to its moderate transparency in the visible and near-infrared (NIR) regions, light harvesting on GO sheets was realized by functionalizing with dye components via noncovalent interactions with the  $\pi$ -surface.<sup>8–15</sup> By this way, the light capture was achieved from the absorption cross-section of the employed photosensitizer. In these hybrid systems, however, the light harvesting was limited by the absorption window of the photosensitizer unit, which indeed corresponds to only a narrow region of the solar irradiance spectrum. There is still demand for new GO hybrid archetypes for effective conversion of solar energy, which can harvest the entire solar output reaching to the Earth surface.

Recently, three-dimensional (3D), ordered assemblies of GO layers functionalized by the bridging building blocks have

drawn much attention due to the possible applications in energy conversion and storage.<sup>16–23</sup> In a recent work, we reported that GO layers formed 3D ordered self-assemblies in the presence of perylenediimides (PDIs) with cationic ammonium substituents (Figure 1a).<sup>18</sup> These assemblies were established through the electrostatic interactions between the cationic groups of PDI and the oxygen functional groups on GO as well as the  $\pi$ – $\pi$  interactions of the large aromatic plane of PDI with the  $\pi$ -conjugations of the GO surface. Photoexcitation of PDIs resulted in very fast electron transfer from GO layers to the PDIs. The results demonstrated that the 3D architecture was necessary for fast charge separation and slow charge recombination; the latter was established by a charge

Received: April 6, 2015

Revised: May 20, 2015

Published: May 21, 2015



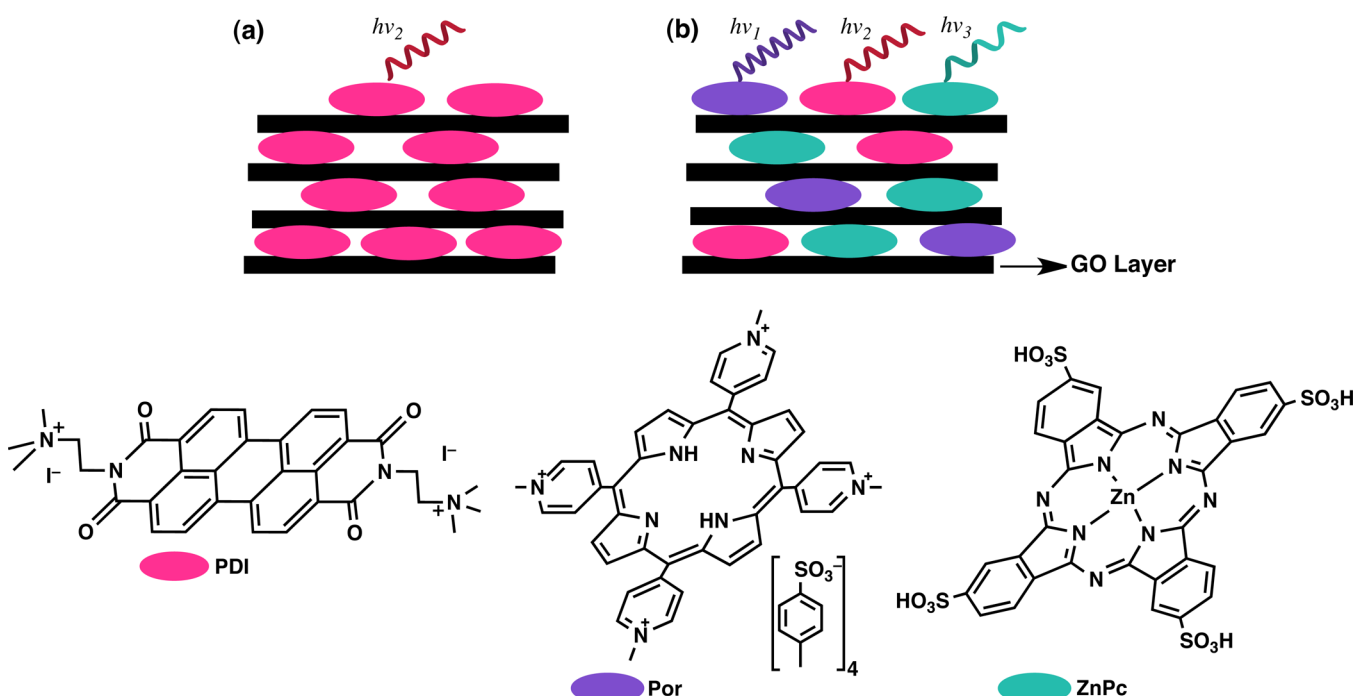


**Figure 1.** (a) Illustration of ordered assemblies of GO–PDI hybrid layers in our previous report.<sup>18</sup> (b) Illustration of proposed self-assemblies GO–Por–PDI–ZnPc hybrid layers with the molecular structures of corresponding compounds used in this study.

migration mechanism taking place between the ordered GO hybrid layers.<sup>18</sup>

In this study, the GO layers were decorated with common redox-active dyes, tetrakis(1-methylpyridinium-4-yl)porphyrin *p*-toluenesulfonate (Por), *N,N'*-di(2-(trimethylammonium iodide)ethylene) perylenediimide (PDI), and Zn(II) phthalocyanine tetrasulfonic acid (ZnPc) with nonoverlapping absorption maxima at around 420, 500, and 620 nm, respectively, for broadband light harvesting (Figure 1b).

Taking the absorption of the GO into the account, the absorption bands of the all components, ceaselessly cover a broad spectral band extending from the ultraviolet (UV) to the NIR regions. Por and PDI bearing cationic groups are expected to trigger assembly of GO layers through the electrostatic and  $\pi$ – $\pi$  interactions in water yielding 3D architectures as observed in our previous report<sup>18</sup> (Figure 1a,b). Anionic ZnPc can have ionic interactions with the cationic units of Por and PDI together with the  $\pi$ – $\pi$  interactions with the GO surface. Photoinduced electron-transfer processes occurring in these hybrid assemblies were studied by using time-resolved laser-induced transient absorption measurements. Photovoltaic features of the self-assemblies were investigated by depositing on nanostructured tin oxide ( $\text{SnO}_2$ ) casted on a transparent electrode.

## 2. EXPERIMENTAL SECTION

**2.1. Materials.** Graphene oxide (GO; as dispersion in water, 4.0 mg mL<sup>-1</sup>; Sigma-Aldrich), tetrakis(1-methylpyridinium-4-yl)porphyrin *p*-toluenesulfonate (Por; TCI), and Zn(II) phthalocyanine tetrasulfonic acid (ZnPc; Frontier Scientific) were used as received. *N,N'*-di(2-(trimethylammonium iodide)-ethylene) perylene diimide (PDI) was synthesized according to reported procedures.<sup>18</sup> Extensive sonication–centrifugation–decantation (SCD) cycles were applied to the samples for

further measurements to completely remove the weakly physiosorbed and nonadsorbed dyes on GO surface.

**2.2. Instruments.** Purification of water (18.2 MΩ cm) was performed with a Milli-Q system (Millipore, Direct-Q 3 UV). Steady-state absorption measurements were recorded on a Hewlett-Packard 8453 diode array spectrophotometer. Powder X-ray diffraction (PXRD) patterns were recorded by a Rigaku Ultima IV. Incident X-ray radiation was produced by Cu X-ray tube, operating at 40 kV and 40 mA with Cu K $\alpha$  radiation of 1.54 Å. A scanning rate was 4° min<sup>-1</sup> from 4° to 50° in 2 $\theta$ . Scanning electron microscopy (SEM) images were taken on a JEOL FE-SEM JSM-6701F instrument operating at 5 kV. Electrochemical measurements were performed on an ALS630B electrochemical analyzer in water containing 0.10 M Na<sub>2</sub>SO<sub>4</sub> as supporting electrolyte. A conventional three-electrode cell was used with a glassy carbon working electrode and a platinum wire as the counter electrode. The measured potentials were recorded with respect to a saturated calomel electrode (SCE). Femtosecond laser-induced transient absorption spectroscopic experiments were conducted using an ultrafast source, Integra-C (Quantronix Corp.); an optical parametric amplifier, TOPAS (Light Conversion Ltd.); and a commercially available optical detection system, Helios provided by Ultrafast Systems LLC. The source for the pump and probe pulses was derived from the fundamental output of Integra-C (780 nm, 2 mJ per pulse and fwhm = 130 fs) at a repetition rate of 1 kHz. Seventy-five percent of the fundamental output of the laser was introduced into TOPAS, which has optical frequency mixers resulting in a tunable range from 285 to 1660 nm, while the rest of the output was used for white light generation. Typically, 2500 excitation pulses were averaged for 3 s to obtain the transient spectrum at a set delay time. Kinetic traces at appropriate wavelengths were assembled from the time-resolved spectral data. Time profiles obtained from femtosecond transient absorption spectra were analyzed by using a computer program, Igor Pro version 6.2. The

formation and decay curves were fitted to a mono and double exponential function of the form  $y = y_0 + A_1 \exp(-t_1^{-1}x) + A_2 \exp(-t_2^{-1}x)$ . Electrophoretic electrode deposition was performed using a Power Pac HV (Bio-Rad). Photoelectrochemical measurements were carried out in a standard two-compartment cell consisting of a working electrode, a Pt wire gauze counter electrode. A KEITHLEY 2400 was used for recording  $I$ - $V$  characteristics and photocurrent generation density under an AM 1.5 simulated light source (OTENTO-SUN II, Bunkoh Keiki Co., Ltd).

### 3. RESULTS AND DISCUSSION

**3.1. Broadband Absorption of Por, PDI, and ZnPc in the Absence of GO.** Proportional distribution of the total absorption of the dye molecules on GO can be provided by mixing in accordance with their molar absorptivities recorded at their absorption maxima ( $\epsilon_{\text{Por}}(422 \text{ nm}) = 214000$ ,  $\epsilon_{\text{PDI}}(501 \text{ nm}) = 36000$ , and  $\epsilon_{\text{ZnPc}}(622 \text{ nm}) = 18400 \text{ M}^{-1} \text{ cm}^{-1}$ )<sup>24</sup> in water. This states a molar ratio of Por, PDI, and ZnPc to be 1:2:12, respectively. Being significantly different than those of individual components,<sup>24</sup> the absorption spectrum of the resulting mixture of these dyes with the indicated molar ratio shows that there exist strong  $\pi$ - $\pi$  interactions among the components initiated by the ionic interactions between the ammonium and pyridinium of PDI and Por with the sulfonic groups of ZnPc (Figure 2).<sup>24,25</sup> Apparently, cationic Por and

electron-rich oxygen functionalities, i.e.,  $-\text{COOH}$  groups, on the GO surface.<sup>17,18</sup> GO layers aggregate after the mixing with the cationic dyes forming self-assembled 3D structures in water.<sup>18</sup> Because the positive and negative charges of dyes have opposite effects on the self-assembly process of the functionalized layers, it is necessary to find a balance among the ratios of Por, PDI, and ZnPc for a complete self-assembly and the proportional distribution of the absorption of each dye component. For this purpose, the dye mixtures having different molar ratios were mixed with the same amount of GO in the same amount of water. By the addition of GO to the dye solution, the initiation of the self-assembly can be recognized from the immediate precipitation. For complete binding and good dispersion of the dyes on the GO surfaces, the mixture was shaken vigorously by hand or by using an automatic lab mixer for a few minutes. After vigorous shaking, the mixtures become viscous (gel-like) depending on the molar ratio of the dyes. To remove the self-assembled GO-dye structures from the nonbinding dye molecules, the mixtures were centrifuged for a few minutes (15000 rpm). The absorption spectra of the dye mixtures before mixing with GO and the supernatants after mixing with GO are shown in Figure 3a–f. Supernatants show the absorption spectra of nonbinding dyes in the solution. It is important to note that mixtures of Por, PDI, and ZnPc at the indicated concentrations do not precipitate upon centrifugation. The absorption of the supernatants in Figure 3a to 3d indicates that the dispersion of the GO layers by the ZnPc molecules is effective; partially preventing the formation of self-assembly aggregates. The decrease in the absorption spectra of Por-PDI-ZnPc in these figures suggests that reasonable amount of dyes doped into the self-assembled GO layers. The complete formation of the self-assembled hybrid layers was recognized when Por, PDI, and ZnPc were mixed in the ratios of 3:2:6 and 1:4:6, respectively, because the supernatants have no realistic absorption in Figure 3e,f. In these cases, the ratios of the cationic “glue” molecules are sufficiently high to compensate the dispersing effect of anionic ZnPc. As a result, the mixtures with high Por and PDI contents tend to form self-assembly aggregates, while the dispersion of functionalized GO layers increases when the ratio of ZnPc is increased. The absorption patterns of Por, PDI, and ZnPc with 1:4:6 ratio are more comparable as compared to those with 3:2:6 ratio, in which the Soret band of Por is exceedingly high.

The supernatants of the mixture with a 1:4:6 molar ratio was treated with different amounts of GO dispersion to examine the effect of the amount of GO on the self-assembly formation. As shown in Figure 4, supernatants of the dye mixtures, treated with 0.20, 0.10, and 0.05 mg of GO, gave no absorption, which indicates the complete self-assembly formation. The amount of dye becomes excess when the amount of GO is lowered to 0.03 mg as understood from the remaining absorption of the supernatant (Figure 4).

Powder X-ray diffraction (PXRD) was utilized to analyze the structural organization in the aggregates of the self-assembled GO layers. The dispersion of GO and the aggregates of the self-assemblies obtained after the centrifugation was dried overnight before the measurements. The dried GO sheets displayed a sharp peak at  $2\theta = 11.96^\circ$  correlated with a  $d$ -spacing of 7.39 Å between the GO layers (Figure 5a).<sup>18,30</sup> The incorporation of dyes with a molar ratio of 1:4:6 into the GO layers increases the  $d$ -spacing to a value of 9.94 Å as the corresponding peak shifts to  $2\theta = 8.89^\circ$  in the PXRD patterns of dried GO-Por-PDI-ZnPc layers (Figure 5b). Average  $d$ -spacing increases by 1.50 Å

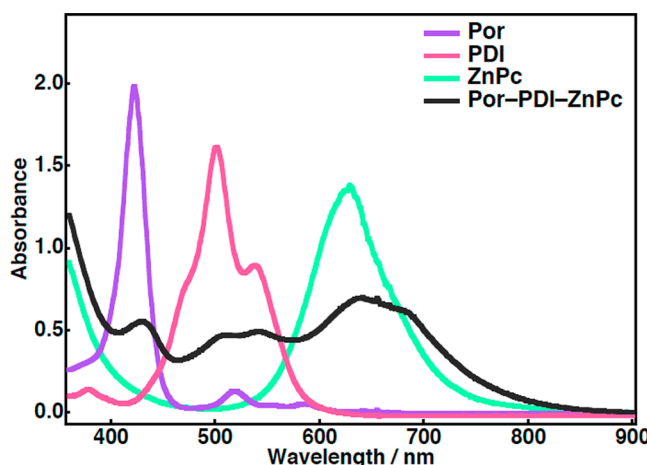


**Figure 2.** Absorption spectra of 0.009 mM Por, 0.05 mM PDI, and 0.074 mM ZnPc and the mixture of 0.008 mM Por, 0.016 mM PDI, and 0.095 mM ZnPc (1:2:12) in water.

PDI and anionic ZnPc form ionic self-assemblies<sup>26</sup> in water in the absence of GO. As expected, the overall absorption of the assemblies of Por, PDI, and ZnPc effectively cover a spectral band from 300 to 900 nm (Figure 2). Absorption patterns of the ionic self-assemblies change as the molar ratio of the components varies (vide infra).

**3.2. Formation of Three-Dimensional Self-Assemblies of GO-Por-PDI-ZnPc.** The binding of the anionic dyes with the large planar aromatic structures to the  $\pi$ -surface of GO through the hydrophobic  $\pi$ - $\pi$  interactions highly improves the dispersion of the graphene and GO layers in aqueous environments due to enhanced electrostatic repulsion by the negative charges,<sup>27–29</sup> whereas the cationic dyes with the adequate aromatic  $\pi$ -planes act as “glue” to combine the GO layers as a result of the electrostatic attractions with the

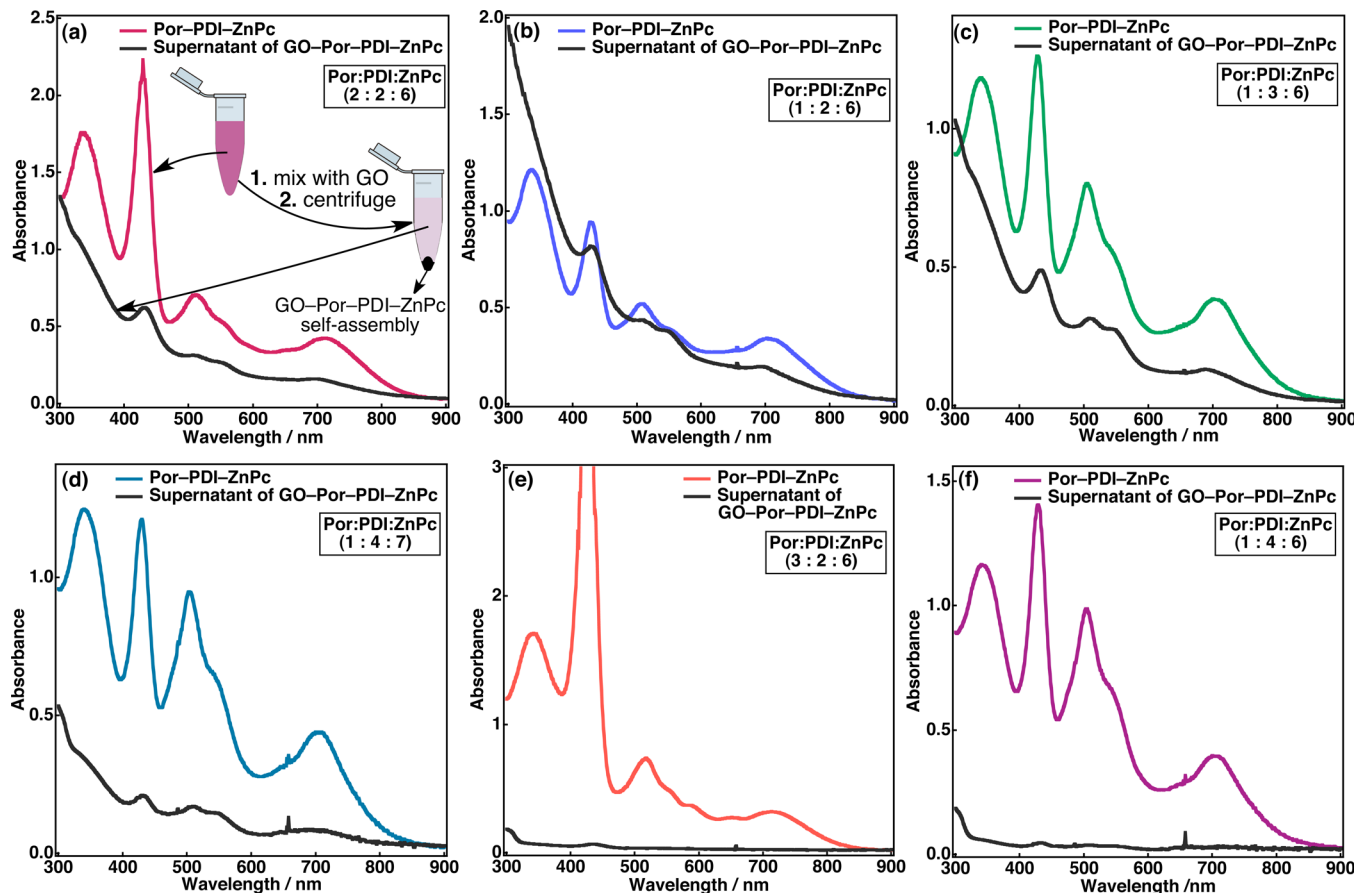


**Figure 3.** Absorption spectra of mixtures of Por, PDI, and ZnPc with the molar ratio of (a) 2:2:6, (b) 1:2:6, (c) 1:3:6, (d) 1:4:7, (e) 3:2:6, and (f) 1:4:6 and the supernatants obtained after mixing with GO (0.2 mg) followed by centrifugation (black line in each figure). The concentration of Por is 0.011 mM when its ratio corresponds to 1 in the mixtures. The inset in panel a summarizes the mixing process repeated for each molar ratio.

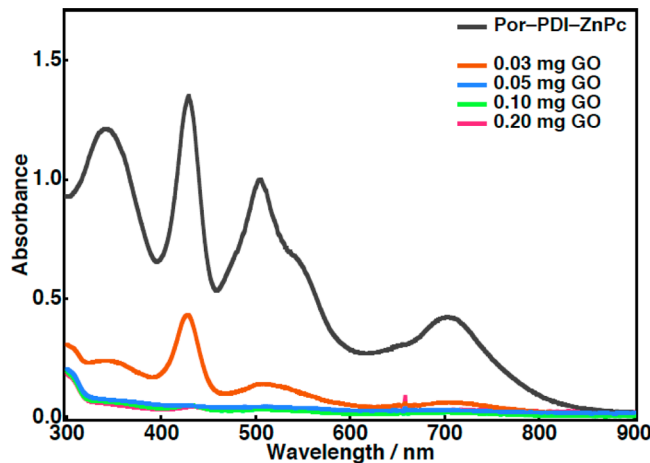


**Figure 4.** Absorption spectra of mixture of Por, PDI, and ZnPc (1:4:6) and the supernatants obtained after mixing with GO at indicated amounts followed by centrifugation.

in the presence of the dye molecules, which is quite the same value (1.55 Å) as obtained by the incorporation of only PDI molecules into GO layers in the previous study.<sup>18</sup> This indicates that instead of extensive cofacial π–π stacking on top of each other, the dye molecules are aligned mostly side by side on the GO surface with a partial stacking assisted by the attraction between the opposite charges and the π–π interactions with the π-conjugations on the GO surface. Such an alignment

provides direct interaction of each component with the GO surface, which may have an effect on electron-transfer processes.

Three-dimensional assemblies of GO–Por–PDI–ZnPc were observed by using scanning electron microscopy (SEM). Top (Figure 6a) and side views (Figure 6b) of the edges of the hybrid samples displayed the ordered stacks of the GO layers in the presence of corresponding dyes, which support the PXRD data. As a result, the insertion of the building blocks having strong interactions with GO is necessary to obtain such 3D structures.<sup>17</sup>

**3.3. Photoinduced Electron-Transfer Processes and Photovoltaic Features of Three-Dimensional Self-Assemblies of GO–Por–PDI–ZnPc.** Femtosecond laser-induced transient absorption spectroscopy was used to monitor the photoinduced events of self-assemblies of GO–Por–PDI–ZnPc taking place in aqueous environments. Self-assemblies of GO decorated by Por, PDI, and ZnPc with a molar ratio of 1:4:6 were excited by laser pulses at 430, 500, and 755 nm, which mainly correspond to the absorption peaks of Por, PDI, and ZnPc, respectively (Figure 2). Excitation at these wavelengths resulted in the same transient traits, which show the ground state bleaching of PDI and ZnPc at around 500 and 700 nm, respectively (Figure 7a–c). Such a broadband bleaching including those of all the components by the excitation of only one component indicates that there is strong electronic communication among the dye molecules. This communication is probably enabled by the partially stacked

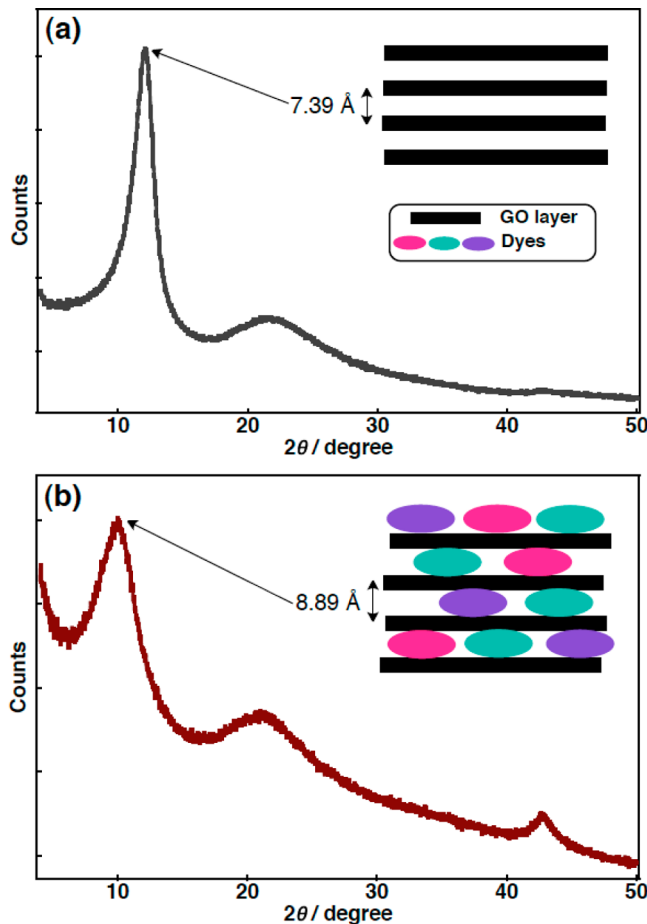


**Figure 5.** Powder X-ray diffraction patterns of dried (a) GO and (b) self-assembly aggregates of GO with Por, PDI, and ZnPc (1:4:6). Inset: Illustrations of GO layers with and without dyes.

alignment of the dye molecules on the  $\pi$ -conjugations of GO layers. The intensity of the bleaching that resulted from the ground state absorption of each component, however, differs as the excitation wavelength changes in each case (Figure 7a–c). The positive absorption appeared with the maxima at 840 and 960 nm in the NIR regions of all spectra can be assigned to the radical cation of ZnPc ( $\text{ZnPc}^{\bullet+}$ ) and the radical anion of PDI ( $\text{PDI}^{\bullet-}$ ), respectively (Figure 7a–c).<sup>31–33</sup> Broadband bleaching of the dyes suppresses the full assignment of the traits of ZnPc and PDI radicals in the visible region. However, the transient bands around 550 (Figure 7a,c) and 650 nm (Figure 7a–c) can be assigned to the absorption of  $\text{ZnPc}^{\bullet+}$  and  $\text{PDI}^{\bullet-}$ , respectively.<sup>18,34</sup> Formation of  $\text{ZnPc}^{\bullet+}$  and  $\text{PDI}^{\bullet-}$  manifests that the charge separation occurs between ZnPc and PDI, regardless of which component is excited. Singlet excited states of all dyes provide sufficient driving force for the photoinduced electron transfer from GO, ZnPc, or Por to PDI as observed in previous studies.<sup>18,35–38</sup> However, ZnPc is the strongest electron donor because of the low first one-electron oxidation potential ( $E_{\text{ox}} = 0.42 \text{ V vs SCE}$ )<sup>34</sup> compared to Por ( $E_{\text{ox}} = 1.09 \text{ V vs SCE}$ ; Figure S1) and GO ( $E_{\text{ox}} = 0.88 \text{ V vs SCE}$ ).<sup>18,39</sup> PDI has a first one-electron reduction potential comparable to that of  $\text{C}_{60}$ ,<sup>40</sup> which is a much stronger electron-acceptor than GO.<sup>41,42</sup> Apparently, GO surface acts as a passage for electrons rather than being a final electron donor or acceptor.<sup>41</sup> Instead, GO accelerates the charge separation by orbital interactions between its  $\pi$ -conjugations and the redox-active dye compo-

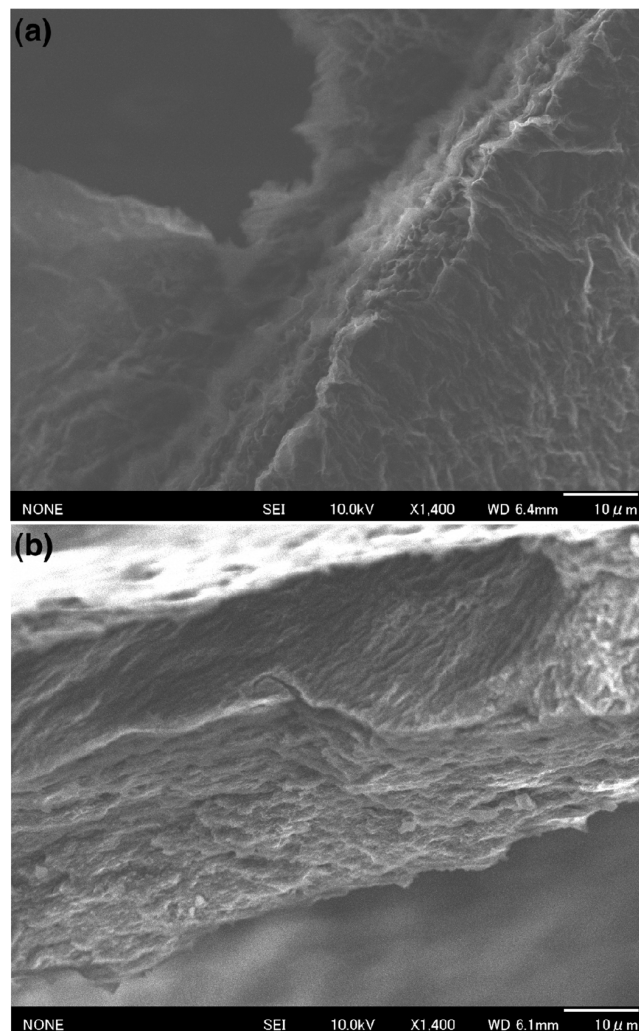


**Figure 6.** SEM images showing the top (a) and side (b) views of the ordered GO hybrid layers obtained from dried aggregates of GO in the presence of Por, PDI, and ZnPc after centrifugation.

nents. Accordingly, excitation of Por is most probably followed by an electron shift to ZnPc molecules directly or through the GO surface. Energy transfer among the dye units seems less likely due to close distance and the highly polar aqueous environment favoring the electron-transfer processes.<sup>43–46</sup> Consequently, there was no signal to be assigned for energy transfer from Por and/or PDI to ZnPc in the transient absorption spectra.<sup>45,46</sup>

The charge separation occurs at less than 1.0 ps as observed in the time profiles at 840 nm (Figure 8a–c). The fast charge separation suggests very high efficiency, ruling out energy transfer mechanisms. The decays at 840 nm corresponds to the charge recombination, which comprises two components, whose lifetime values are extracted by fitting with use of a sum of two decaying exponentials (Figure 8a–c). The first components of the fitting curves gave lifetimes for the first charge recombination as 17, 21, and 22 ps, respectively, while the lifetimes of the final charge recombination were evaluated as 141, 204, and 220 ps, respectively, when Por, PDI, and ZnPc are respectively excited at 435 (Figure 8a), 500 (Figure 8b), and 755 nm (Figure 8c). The lifetime values obtained from the decay at 960 nm were quite comparable to these data. The two-component decay of the radical ions was also observed in

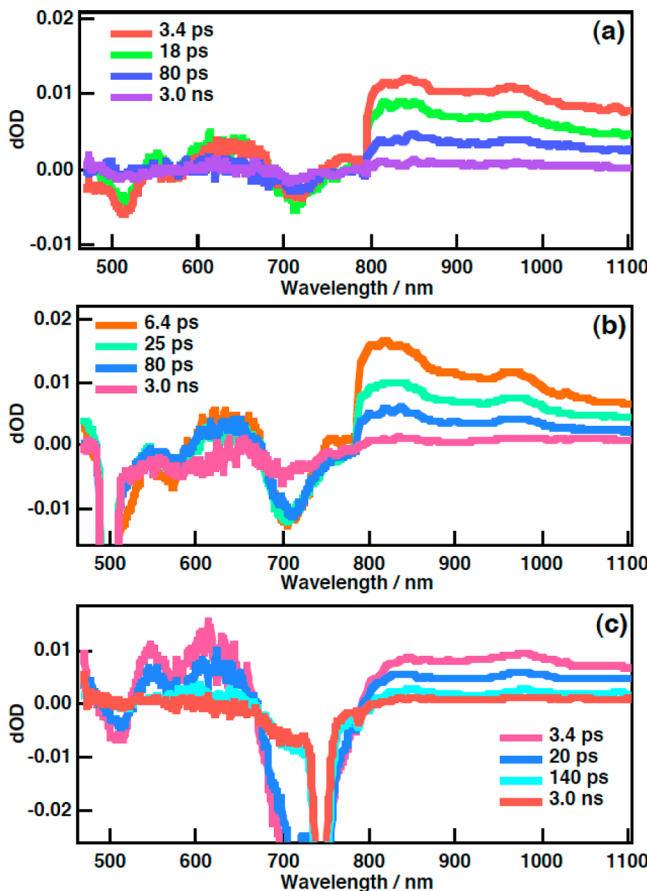


**Figure 7.** Femtosecond laser-induced transient absorption spectra of self-assembly aggregates of GO with Por, PDI, and ZnPc (1:4:6) excited at (a) 430, (b) 500, and (c) 755 nm, respectively.

previous polymeric self-assemblies, and the slow component was interpreted for the charge migration along the stacked molecules.<sup>24,47</sup> The lifetime value for charge recombination is smaller than that observed in the 3D assemblies of GO and PDI (417 ps), in which the GO was the final electron donor, which was actively involved in interlayer charge migration.<sup>18</sup> In this case, as the molar ratio of the excited dye increases the charge recombination becomes slower. Also, increasing the amount of GO does not have a significant effect on the charge separation and recombination kinetics. These results suggest that vertical (interlayer) charge migration through the GO layers in this hybrid system is not effective. Nonetheless, the two-component decay indicates a lateral charge migration among the partially stacked dye molecules aligned on a GO layer.

To determine the response of the self-assemblies of dye functionalized GO layers toward the photocurrent and photovoltage generation, their aggregates were deposited on an optically transparent electrode (OTE) of nanostructured SnO<sub>2</sub> (OTE/SnO<sub>2</sub>-(GO-Por-PDI-ZnPc)<sub>n</sub>) and compared with those of only Por-PDI-ZnPc (OTE/SnO<sub>2</sub>-(Por-PDI-ZnPc)<sub>n</sub>) and only GO (OTE/SnO<sub>2</sub>-(GO)<sub>n</sub>) deposited on OTE of SnO<sub>2</sub> in the electrolyte system (Figure 9a,b and Figure S2). The procedures, described for the electrode fabrication of the previous hybrid systems that we studied, were also applied in this study (see also Experimental Section).<sup>48–51</sup> The responses of OTE/SnO<sub>2</sub>-(GO-Por-PDI-ZnPc)<sub>n</sub> and OTE/SnO<sub>2</sub>-(Por-PDI-ZnPc)<sub>n</sub> were steady and reproducible during the repeated on/off cycles of the visible light

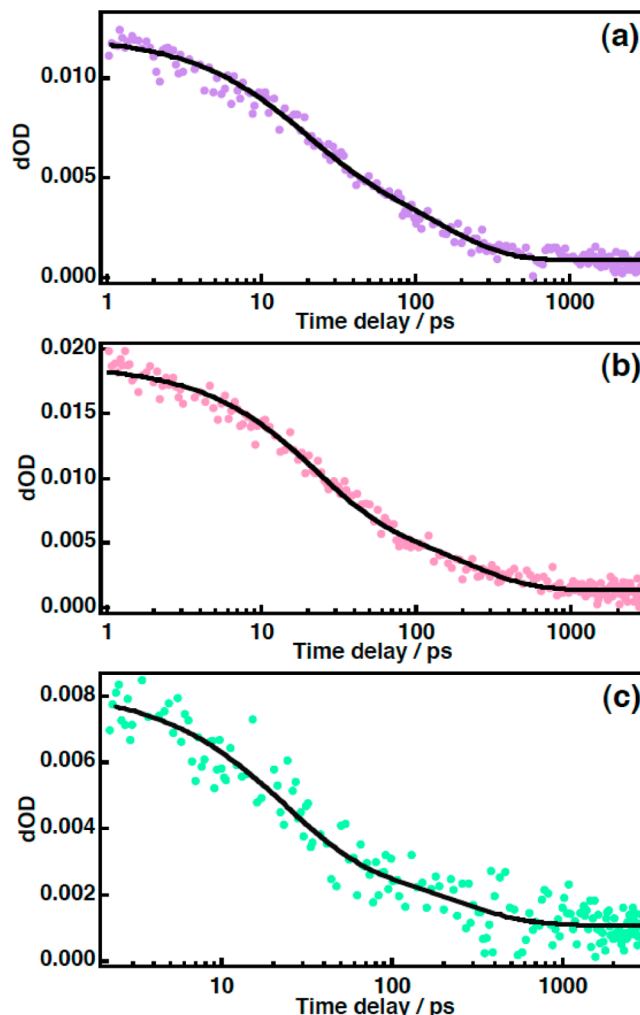


**Figure 8.** Time profile showing the decay of ZnPc\*<sup>+</sup> at 840 nm in the self-assembly aggregates of GO with Por, PDI, and ZnPc (1:4:6) under the photoexcitation at (a) 430, (b) 500, and (c) 755 nm, respectively.

illumination, whereas the electrode deposited with only GO produced no detectable photocurrent. The photocurrent (Figure 9a) and the photovoltage responses (Figure 9b) were markedly enhanced on OTE/SnO<sub>2</sub> electrode deposited with the self-assemblies of GO-Por-PDI-ZnPc compared to that deposited with only dye molecules.<sup>48</sup> Such enhancement demonstrates that the initiation of photocurrent generation by photoinduced charge separation<sup>49–51</sup> occurs in the GO-Por-PDI-ZnPc followed by a charge migration process among the dye molecules aligned on the GO layers as detected by the femtosecond transient absorption measurements.

#### 4. CONCLUSIONS

To conclude, ordered assemblies of GO layers were constructed by the functionalization with cationic Por and PDI and anionic ZnPc dyes. Combination of the dye components resulted in broadband light harvesting as indicated by the ceaseless absorption window extending from UV to NIR region. Proper molar balance between the cationic dyes combining the GO layers through electrostatic attractions and the anionic dyes acting as dispersants of GO layers is necessary to obtain robust 3D assembly structures. Dye molecules are aligned laterally with partial stacking between the GO layers, providing direct interaction with the  $\pi$ -patterns of the GO

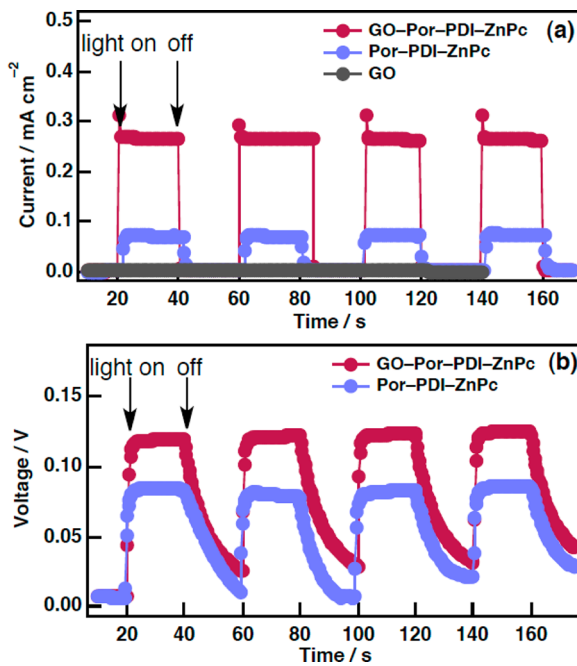


**Figure 9.** (a) Photocurrent and (b) photovoltage responses of corresponding components deposited on OTE/SnO<sub>2</sub> electrodes under white light illumination ( $100 \text{ mW cm}^{-2}$ ). Electrolyte: 0.5 M LiI and 0.01 M I<sub>2</sub> in MeCN.

surface. Self-assembly in 3D facilitates very fast charge separation upon photoexcitation of the dyes at various wavelengths in the visible/NIR region. GO layers accelerate the charge separation between the final donor and acceptor, i.e., ZnPc and PDI. Lateral charge migration among the partially stacked dye molecules was deduced from the decay characteristics of the generated radical ion pair of ZnPc and PDI, which led to slow charge recombination. Lastly, incorporation of light harvesting dyes into GO layers significantly enhanced the photocurrent generation of the OTE/SnO<sub>2</sub> electrode loaded with self-assemblies of GO–Por–PDI–ZnPc.

## ■ ASSOCIATED CONTENT

### Supporting Information

Figures S1 and S2: DPV voltammogram and  $I$ – $V$  characteristics. The Supporting Information is available free of charge on the ACS Publications website at DOI: 10.1021/acs.jpcc.5b03303.

## ■ AUTHOR INFORMATION

### Corresponding Author

\*E-mail: fukuzumi@chem.eng.osaka-u.ac.jp. Tel: +81-6-6879-7368. Fax: +81-6-6879-7370.

### Notes

The authors declare no competing financial interest.

## ■ ACKNOWLEDGMENTS

This work was supported by ALCA and SENTAN program from the Japan Science Technology Agency (JST) to S.F.; a Grant-in-Aid (Nos. 26620154 and 26288037 to K.O., Nos. 26286017 and 26620159 to T.H.) and JSPS fellowships to M.S. (PD) and to Y.K. (25·727, DC1) from MEXT, Japan.

## ■ REFERENCES

- Chen, D.; Feng, H.; Li, J. Graphene Oxide: Preparation, Functionalization, and Electrochemical Applications. *Chem. Rev.* **2012**, *112*, 6027–6053.
- Huang, X.; Qi, X.; Boey, F.; Zhang, H. Graphene-Based Composites. *Chem. Soc. Rev.* **2012**, *41*, 666–686.
- Lightcap, I. V.; Kamat, P. V. Graphitic Design: Prospects of Graphene-Based Nanocomposites for Solar Energy Conversion, Storage, and Design. *Acc. Chem. Res.* **2013**, *46*, 2235–2243.
- Chang, H.; Wu, H. Graphene-Based Nanocomposites: Preparation, Functionalization, and Energy and Environmental Applications. *Energy Environ. Sci.* **2013**, *6*, 3483–3507.
- Tang, Q.; Zhou, Z.; Chen, Z. Graphene-Related Nanomaterials: Tuning Properties by Functionalization. *Nanoscale* **2013**, *5*, 4541–4583.
- D'Souza, F.; Ito, O. Photoinduced Electron Transfer Processes of Functionalized Nanocarbons; Fullerenes, Nanotubes and Graphene. *Sci. Prog.* **2013**, *96*, 369–397.
- Yin, Z.; Zhu, J.; He, Q.; Cao, X.; Tan, C.; Chen, H.; Yan, Q.; Zhang, H. Graphene-Based Materials for Solar Cell Applications. *Adv. Energy Mater.* **2014**, *4*, 1300574.
- Geng, J.; Jung, H.-T. Porphyrin Functionalized Graphene Sheets in Aqueous Suspension: From the Preparation of Graphene Sheets to Highly Conductive Graphene Films. *J. Phys. Chem. C* **2010**, *114*, 8227–8234.
- Wojcik, A.; Kamat, P. V. Reduced Graphene Oxide and Porphyrin. An Interactive Affair in 2-D. *ACS Nano* **2010**, *4*, 6697–6706.
- Bikram K. C., C.; Das, S. K.; Ohkubo, K.; Fukuzumi, S.; D'Souza, F. Ultrafast Charge Separation in Supramolecular Tetrapyrrole–Graphene Hybrids. *Chem. Commun.* **2012**, *48*, 11859–11861.
- Liu, Z. D.; Zhao, H. X.; Huang, C. Z. Obstruction of Photoinduced Electron Transfer from Excited Porphyrin to Graphene Oxide: A Fluorescence Turn-On Sensing Platform for Iron(III) Ions. *PLoS One* **2012**, *7*, e50367 DOI: 10.1371/journal.pone.0050367.
- Skaltsas, T.; Pispas, S.; Tagmatarchis, N. Photoinduced Charge-Transfer Interactions on a Graphene/Block Copolymer Electrostatically Bound to Tetracationic Porphyrin in Aqueous Media. *Chem.–Eur. J.* **2013**, *19*, 9286–9290.
- Kiessling, D.; Costa, R. D.; Katsukis, G.; Malig, J.; Lodermeier, F.; Feihl, S.; Roth, A.; Wibmer, L.; Kehrer, M.; Volland, M.; et al. Novel Nanographene/Porphyrin Hybrids—Preparation, Characterization, and Application in Solar Energy Conversion Schemes. *Chem. Sci.* **2013**, *4*, 3085–3098.
- An, N.; Zhang, F.; Hu, Z.; Li, Z.; Li, L.; Yang, Y.; Guo, B.; Lei, Z. Non-Covalently Functionalizing a Graphene Framework by Anthraquinone for High-Rate Electrochemical Energy Storage. *RSC Adv.* **2015**, *5*, 23942–23951.
- Economopoulos, S. P.; Tagmatarchis, N. Multichromophores Onto Graphene: Supramolecular Non-Covalent Approaches for Efficient Light Harvesting. *J. Phys. Chem. C* **2015**, *119*, 8046–8053.
- Yuan, J.; Zhu, J.; Bi, H.; Meng, X.; Liang, S.; Zhang, L.; Wang, X. Graphene-Based 3D Composite Hydrogel by Anchoring Co<sub>3</sub>O<sub>4</sub> Nanoparticles with Enhanced Electrochemical Properties. *Phys. Chem. Chem. Phys.* **2013**, *15*, 12940–12945.
- Srinivasan, S.; Je, S. H.; Back, S.; Barin, G.; Buyukcakir, O.; Guliyev, R.; Jung, Y.; Coskun, A. Ordered Supramolecular Gels Based on Graphene Oxide and Tetracationic Cyclophanes. *Adv. Mater.* **2014**, *26*, 2725–2729.
- Supur, M.; Ohkubo, K.; Fukuzumi, S. Photoinduced Charge Separation in Ordered Self-Assemblies of Perylenediimide–Graphene Oxide Hybrid Layers. *Chem. Commun.* **2014**, *50*, 13359–13361.
- Gan, S.; Zhong, L.; Engelbrekt, C.; Zhang, J.; Han, D.; Ulstrup, J.; Chi, Q.; Niu, L. Graphene Controlled H- and J-Stacking of Perylene Dyes into Highly Stable Supramolecular Nanostructures for Enhanced Photocurrent Generation. *Nanoscale* **2014**, *6*, 10156–10523.
- Song, S.; Xue, Y.; Feng, L.; Elbatal, H.; Wang, P.; Moorefield, C. N.; Newcome, G. R.; Dai, L. Reversible Self-Assembly of Terpyridine-

- Functionalized Graphene Oxide for Energy Conversion. *Angew. Chem., Int. Ed.* **2014**, *53*, 1415–1419.
- (21) Cao, X.; Yin, Z.; Zhang, H. Three-Dimensional Graphene Materials: Preparation, Structures and Application in Supercapacitors. *Energy Environ. Sci.* **2014**, *7*, 1850–1865.
- (22) Chen, L.; Feng, M.; Zhan, H. Fundamental Electrochemistry of Three-Dimensional Graphene Aerogels. *RSC Adv.* **2014**, *4*, 30689–30696.
- (23) Wang, Z.; Hu, G.; Liu, J.; Liu, W.; Zhang, H.; Wang, B. Coordinated Assembly of a New 3D Mesoporous  $\text{Fe}_3\text{O}_4@\text{Cu}_2\text{O}$ –Graphene Oxide Framework as a Highly Efficient and Reusable Catalyst for the Synthesis of Quinoxalines. *Chem. Commun.* **2015**, *51*, S069–S072.
- (24) Similar to PDI, ZnPc forms solubilized  $\pi$ -stacks, while Por dissolves as monomers in water. See: Supur, M.; Fukuzumi, S. Photodriven Electron Transport within the Columnar Perylenediimide Nanostructures Self-assembled with Sulfonated Porphyrins in Water. *J. Phys. Chem. C* **2012**, *116*, 23274–23282.
- (25) Guan, Y.; Yu, S.-H.; Antonietti, M.; Böttcher, C.; Faul, C. F. J. Synthesis of Supramolecular Polymers by Ionic Self-Assembly of Oppositely Charge Dyes. *Chem.—Eur. J.* **2005**, *11*, 1305–1311.
- (26) Faul, C. F. J. Ionic Self-Assembly for Functional Hierarchical Nanostructured Materials. *Acc. Chem. Res.* **2014**, *47*, 3428–3438.
- (27) Su, Q.; Pang, S.; Alijani, V.; Li, C.; Feng, X.; Müllen, K. Composites of Graphene with Large Aromatic Molecules. *Adv. Mater.* **2009**, *21*, 3191–3195.
- (28) Jiang, B.-P.; Hu, L.-F.; Wang, D.-J.; Ji, S.-C.; Shen, X.-C.; Liang, H. Graphene Loading Water-Soluble Phthalocyanine for Dual-Modality Photothermal/Photodynamic Therapy via a One-Step Method. *J. Mater. Chem. B* **2014**, *2*, 7141–7148.
- (29) Zhang, X.-F.; Shao, X.  $\pi$ - $\pi$  Binding Ability of Different Carbon Nano-Materials with Aromatic Phthalocyanine Molecules: Comparison between Graphene, Graphene Oxide and Carbon Nanotubes. *J. Photochem. Photobiol., A* **2014**, *278*, 69–74.
- (30) In a previous study, we reported the  $d$ -spacing value for another GO as 8.66 Å. The variation should be due to the difference in the oxidation process used for the chemical exfoliation of graphite.
- (31) Fukuzumi, S.; Ohkubo, K.; Ortiz, J.; Gutiérrez, A. M.; Fernández-Lázaro, F.; Sastre-Santos, Á. Formation of a Long-Lived Charge Separated State of a Zinc Phthalocyanine–Perylenediimide Dyad by Complexation with Magnesium Ion. *Chem. Commun.* **2005**, 3814–3816.
- (32) Fukuzumi, S.; Ohkubo, K.; Ortiz, J.; Gutiérrez, A. M.; Fernández-Lázaro, F.; Sastre-Santos, Á. Control of Photoinduced Electron Transfer in Zinc Phthalocyanine–Perylenediimide Dyad and Triad by the Magnesium Ion. *J. Phys. Chem. A* **2008**, *112*, 10774–10752.
- (33) Supur, M.; Yamada, Y.; El-Khouly, M.; Honda, T.; Fukuzumi, S. Electron Delocalization in One-Dimensional Perylenediimide Nanobelts through Photoinduced Electron Transfer. *J. Phys. Chem. C* **2011**, *115*, 15040–15047.
- (34) Jin, S.; Ding, X.; Feng, X.; Supur, M.; Furukawa, K.; Takahashi, S.; Addicoat, M.; El-Khouly, M. E.; Nakamura, T.; Irle, S.; et al. Charge Dynamics in a Donor–Acceptor Covalent Organic Framework with Periodically Ordered Bicontinuous Heterojunctions. *Angew. Chem., Int. Ed.* **2013**, *52*, 2017–2021.
- (35) Chen, Y.; Lin, Y.; El-Khouly, M. E.; Zhuang, Z.; Araki, Y.; Ito, O.; Zhang, W. Supramolecular Zinc Phthalocyanine–Perylene Bisimide Triad: Synthesis and Photophysical Properties. *J. Phys. Chem. C* **2007**, *111*, 16096–16099.
- (36) Jimenez, Á. J.; Spänig, F.; Rodriguez-Morgade, M. S.; Ohkubo, K.; Fukuzumi, S.; Guldi, D. M.; Torres, T. A Tightly Coupled Bis(zinc(II) phthalocyanine)–Perylenediimide Ensemble to Yield Long-Lived Radical Ion Pair States. *Org. Lett.* **2007**, *9*, 2481–2484.
- (37) Cespedes-Guirao, F. J.; Ohkubo, K.; Fukuzumi, S.; Sastre-Santos, Á.; Fernandez-Lazaro, F. Synthesis and Photoinduced Electron Transfer of Phthalocyanine–Perylenebisimide Pentameric Arrays. *J. Org. Chem.* **2009**, *74*, 5871–5880.
- (38) Suzuki, S.; Kozaki, M.; Nozaki, K.; Okada, K. Recent Progress in Controlling Photophysical Processes of Donor–Acceptor Arrays Involving Perylene Diimides and Boron-Dipyrromethenes. *J. Photochem. Photobiol., C* **2011**, *12*, 269–292.
- (39) Oxidation potential of GO can vary with the degree of oxidation of reactant graphite during the synthesis of GO. See: Krishnamoorthy, K.; Veerapandian, M.; Yun, K.; Kim, S.-J. The Chemical and Structural Analysis of Graphene Oxide with Different Degrees of Oxidation. *Carbon* **2013**, *53*, 38–49.
- (40) Supur, M.; Fukuzumi, S. Energy and Electron Transfer of One-Dimensional Nanomaterials of Perylenediimides. *ECS J. Solid State Sci. Technol.* **2013**, *2*, M3051–M3062.
- (41) Das, S. K.; KC, C. B.; Ohkubo, K.; Yamada, Y.; Fukuzumi, S.; D’Souza, F. Decorating Single Layer Graphene Oxide with Electron Donor and Acceptor Molecules for the Study of Photoinduced Electron Transfer. *Chem. Commun.* **2013**, *49*, 2013–2015.
- (42) Karousis, N.; Ortiz, J.; Ohkubo, K.; Hasobe, T.; Fukuzumi, S.; Sastre-Santos, Á.; Tagmatarchis, N. Zinc Phthalocyanine–Graphene Hybrid Material for Energy Conversion: Synthesis, Characterization, Photophysics, and Photoelectrochemical Cell Preparation. *J. Phys. Chem. C* **2012**, *116*, 20564–20573.
- (43) Supur, M.; Yamada, Y.; Fukuzumi, S. Excitation Energy Transfer from Non-Aggregated Molecules to Perylenediimide Nanoribbons via Ionic Interactions in Water. *J. Mater. Chem.* **2012**, *22*, 12547–12552.
- (44) Supur, M.; Sung, Y. M.; Kim, D.; Fukuzumi, S. Enhancement of Photodriven Charge Separation by Conformational and Intermolecular Adaptations of an Anthracene–Perylenediimide–Anthracene Triad to an Aqueous Environment. *J. Phys. Chem. C* **2013**, *117*, 12438–12445.
- (45) KC, C. B.; Ohkubo, K.; Karr, P. A.; Fukuzumi, S.; D’Souza, F. A ‘Two-Point’ Bound Zinc Porphyrin–Zinc Phthalocyanine–Fullerene Supramolecular Triad for Sequential Energy and Electron Transfer. *Chem. Commun.* **2013**, *49*, 7614–7616.
- (46) KC, C. B.; Lim, G. N.; Karr, P. A.; D’Souza, F. Supramolecular Tetrad Featuring Covalently Linked Bis(porphyrin)–Phthalocyanine Coordinated to Fullerene: Construction and Photochemical Studies. *Chem.—Eur. J.* **2014**, *20*, 7725–7735.
- (47) Supur, M.; Fukuzumi, S. Tuning the Photodriven Electron Transport within the Columnar Perylenediimide Stacks by Changing the  $\pi$ -Extent of the Electron Donors. *Phys. Chem. Chem. Phys.* **2013**, *15*, 2539–2546.
- (48) GO oxide showed negligible photovoltage response when deposited on OTE of  $\text{SnO}_2$  in the electrolyte system under the same conditions in a recent study. See: Supur, M.; Kawashima, Y.; Ohkubo, K.; Sakai, H.; Hasobe, T.; Fukuzumi, S. Graphene Oxide– $\text{Li}^+@\text{C}_{60}$  Donor–Acceptor Composite for Photoenergy Conversion. *Phys. Chem. Chem. Phys.* **2015**, DOI: 10.1039/C5CP01403D.
- (49) Ohkubo, K.; Kawashima, Y.; Sakai, H.; Hasobe, T.; Fukuzumi, S. Enhanced Photoelectrochemical Performance of Composite Photovoltaic Cells of  $\text{Li}^+@\text{C}_{60}$ –Sulphonated Porphyrin Supramolecular Nanoclusters. *Chem. Commun.* **2013**, *49*, 4474–4476.
- (50) Ohkubo, K.; Kawashima, Y.; Mase, K.; Sakai, H.; Hasobe, T.; Fukuzumi, S. Photoelectrochemical Properties of Supramolecular Composites of an Anionic Zinc Chlorin and  $\text{Li}^+@\text{C}_{60}$  on  $\text{SnO}_2$ . *J. Porphyrins Phthalocyanines* **2014**, *18*, 982–990.
- (51) Kawashima, Y.; Ohkubo, K.; Blas-Fernando, V. M.; Sakai, H.; Font-Sanchis, E.; Ortiz, J.; Fernández-Lázaro, F.; Hasobe, T.; Sastre-Santos, Á.; Fukuzumi, S. Near-Infrared Photoelectrochemical Conversion via Photoinduced Charge Separation in Supramolecular Complexes of Anionic Phthalocyanines with  $\text{Li}^+@\text{C}_{60}$ . *J. Phys. Chem. B* **2015**, DOI: 10.1021/jp5123163.